JOURNAL OF AGRICULTURAL AND FOOD CHEMISTRY

Open Access

pubs.acs.org/JAFC

Article

Crystal Structure of Autophagy-Associated Protein 8 at 1.36 Å Resolution and Its Inhibitory Interactions with Indole Analogs

Shanqi Zhang, Xin Luo, Xiu Yuan, Danxia Wu, Jing Liu, Kunhong Zhao, Youwei Xu, Jingjiang Zhou, Xiangyang Li,* and Qing X. Li*

Cite This: *J. Agric. Food Chem.* 2025, 73, 7111−7120

Read Online

ACCESS | Metrics & More | Article Recommendations | Supporting Information

ABSTRACT: Autophagy-associated protein 8 (ATG8) is essential for autophagy and organismal growth and development. In this study, we successfully resolved the crystal structure of *Drosophila melanogaster* (*D. melanogaster*) ATG8a (*Dm*ATG8a) at 1.36 Å resolution. Being distinct from previously characterized ATG8 homologues, *Dm*ATG8a (121 residues) adopts a unique fold comprising five α-helices and four β-folding strands, in contrast to the canonical four α-helices and four β-folding strands observed in other ATG8 proteins. *Dm*ATG8a features two active cavities: hydrophobic pocket 1 (HP1) and hydrophobic pocket 2 (HP2), which are essential for the normal physiological function of ATG8. Indole and its analogs can bind specifically with HP1. Microscale thermophoresis results demonstrated a strong affinity of 6-fluoroindole with *Dm*ATG8a (3.54 μmol/L), but no affinity with the *Dm*ATG8a^{K48A} mutant, suggesting that Lys48 is critical in binding 6-fluoroindole probably via a hydrogen bond interaction. The half-maximum lethal concentration (LC_{50}) of 6-fluoroindole against *D. melanogaster* adult flies was 169 μg/mL. Our findings establish *Dm*ATG8a as a promising target for developing indole-based insecticides.

KEYWORDS: *ATG8a, DmATG8a, Drosophila melanogaster, 6-fluoroindole, insecticide*

INTRODUCTION

Food demand is growing to meet the continuous increase in the global human population.[1] Pest insects cause huge losses in food production every year. Not only do they directly damage plants, but many of them also act as vectors for plant viruses, posing a significant threat to agricultural production.[2,3] Among various insect control methods such as genetically modified plants and microbial agents,[4,5] insecticides have been the dominant method due to their advantages including rapid effectiveness and predictability. However, excessive insecticide application has led to widespread resistance in pest populations, drastically diminishing control efficacy. Resistance not only undermines the efficacy of existing insecticides but also induces cross-resistance to newly developed insecticides with the same molecular targets. Under such circumstances, pest control is frequently attempted through increased insecticide application rates, which seriously pollutes the environment. To address the resistance and pollution challenges, it is therefore of great interest to develop new insecticidal targets to better control pest insects.

The autophagy-associated protein 8 (ATG8) was identified from a human brain cDNA library.[6] ATG8 is crucial for the physiological function of γ-aminobutyric acid subtype A receptors ($GABA_A$ receptors). Research has demonstrated that ATG8 promotes the aggregation of $GABA_A$ receptors, enhancing the electrical signals generated by these receptors, and thus influencing the dynamics of gated ion channels.[7−10]

In addition to its close relationship with $GABA_A$ receptor function, ATG8 is critical for autophagy. This dual role of ATG8 in autophagy and neurotransmission underscores its potential as a multifunctional therapeutic target. ATG8 is the most common marker of autophagy. It belongs to the ubiquitin-like family of proteins and is integral to the autophagic process.[11] Autophagy represents a conserved and meticulously regulated intracellular process for the degradation of materials in eukaryotic organisms.[12−14] It is typically categorized into three types, macroautophagy, microautophagy, and molecular chaperone-mediated autophagy.[15,16] Macroautophagy is the most studied among the three types of autophagy. A defining characteristic of macroautophagy is the formation of autophagic vesicles with a double-layer membrane structure. Studies have indicated that the formation of these vesicles may be associated with the outer membrane of the mitochondria, the membrane of the endoplasmic reticulum, and the plasma membrane.[17−19] In the macroautophagy pathway, ATG8 is synthesized as pro-proteins cleaved by ATG4 to expose glycine residues,[20,21] the newly exposed C-terminal glycine carboxyl group is linked to a cysteine of ATG7 via a thioester bond. Subsequently ATG8 is transferred from ATG7 to ATG3, which binds ATG8 via a thioester bond.[22−24] Finally, in the presence of the ATG12-ATG5 complex, ATG3 is released and ATG8 is coupled to the amino group of phosphatidylethanolamine (PE) via an amide bond to form a ATG8-PE conjugate, which can mediate the membrane fusion events necessary for autophagosome bio-

Received: November 14, 2024
Revised: February 27, 2025
Accepted: February 28, 2025
Published: March 11, 2025

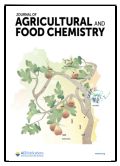

https://doi.org/10.1021/acs.jafc.4c11205
J. Agric. Food Chem. 2025, 73, 7111−7120

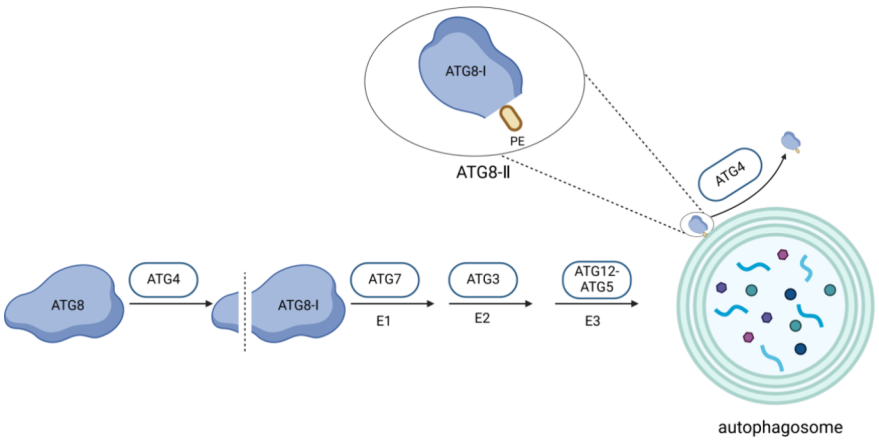

Figure 1. Involvement of autophagy-associated protein 8 (ATG8) family proteins in the macroautophagy pathway. PE, phosphatidylethanolamine; E1, ubiquitin-activating enzyme; E2, ubiquitin-conjugating enzyme; E3, ubiquitin-protein ligase; ATG8-I, a form of ATG8 formed after cleavage of the amino acid residues at the C-terminal glycine (116G) of ATG8; ATG8-II, a form of ATG8 after the C-terminal glycine residue of ATG8-I is esterified with phosphatidylethanolamine (PE).

genesis.[25] The ATG8-PE conjugate is predominantly located on both sides of the autophagic vesicle membrane, and ATG4 removes ATG8-PE from the outer membrane as the autophagosome matures (Figure 1).[20,26]

The number of ATG8 proteins varies among different species. For instance, yeast contains only one ATG8 gene, while mammals possess seven ATG8 homologues, which can be classified into two subfamilies according to similarities in their amino acid sequences: the LC3 subfamily and the GABARAP subfamily.[27] Most reported studies on ATG8 have primarily focused on mammals, with relatively few investigations on insects.

Drosophila melanogaster is a well-studied model organism that has contributed greatly to the discovery of drugs and the identification of drug targets.[28,29] ATG8 is crucial for the growth and development of *D. melanogaster*. As a core component of autophagy, it can regulate cell remodeling and tissue reconstruction and participate in the transformation process from larvae to pupae and from pupae to adults.[30]

There are two ATG8 homologues in *D. melanogaster*, ATG8a and ATG8b, of which only ATG8a is essential for autophagosome development.[31] *Dm*ATG8a is categorized within the GABARAP subfamily. Under starvation, the mRNA levels of *Dm*ATG8a are upregulated, while *Dm*ATG8b mRNA level remains unchanged. When ATG8a is deficient in *D. melanogaster*, it leads to a series of problems, such as partial lethality, abnormal wings, shortened lifespan, decreased climbing ability, reduced muscle integrity, and progressive degeneration of the nervous system, which severely affect the normal physiological activities of *D. melanogaster*.[32]

ATG8 family proteins have been recognized as potential drug targets across various species. For example, Wool et al. (2024) demonstrated that ebselen and its analogs can inhibit the interaction between ATG4 and ATG8, significantly reducing the pathogenicity of the fungi *Botrytis cinerea* and *Magnaporthe oryzae*.[33] Similarly, Wang et al. (2022) found that methyl eugenol binds ATG8, indicating that ATG8 could be a promising molecular action target.[34] Thielmann et al. (2008) reported that 94% of the peptide chains that interacted with ATG8 contained tryptophan residues.[35] It was hypothesized that the tryptophan residues in the peptides are crucial for their interactions with ATG8, providing a structural basis for the development of ATG8 inhibitors. Indoles share structural similarities with tryptophan, featuring a backbone that forms a common aromatic heterocycle present in numerous organisms, encompassing plants, animals, and marine species. Indole derivatives can bind multiple receptors and exhibit diverse biological activities, including insecticidal,[36,37] antiviral,[38] and antibacterial effects.[39]

In this study, we expressed the ATG8a protein from the *D. melanogaster* gene with *Escherichia coli* and the crystal structure was elucidated at a resolution of 1.36 Å. We screened a series of indole analogs using microscale thermophoresis (MST). For those with strong binding abilities, we determined the binding site through molecular docking and mutagenesis experiments. Finally, we evaluated the insecticidal activity of these compounds against *D. melanogaster*. Our results provide insights into the molecular interactions between ATG8 and small indole molecules and lay a foundation for future design of insecticides targeting the ATG8 family of proteins.

MATERIALS AND METHODS

Chemical Reagents. Haloindoles and tryptophan (Figure 2) with analytical purity were procured from Aladdin, Shanghai Reagent Company, China. All compounds were stored at 4 °C.

Plasmid. The pET32a-*Dm*ATG8a plasmid was obtained from Beijing Tsingke Biotech Co., Ltd. The amino acid sequence of *Dm*ATG8a is from the NCBI database (https://www.ncbi.nlm.nih.gov/). The *Dm*ATG8a gene was digested with NdeI and XhoI and then inserted into the pET-32a vector.

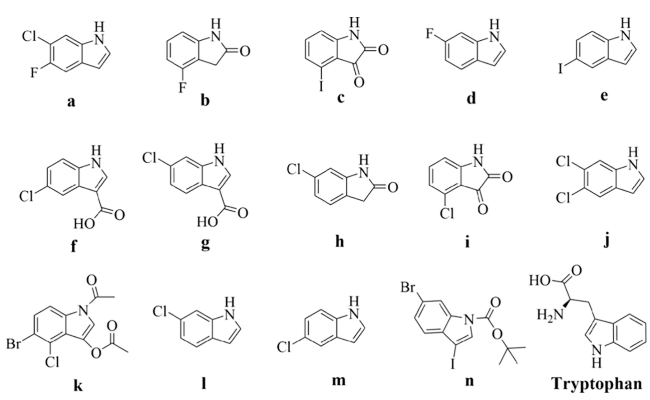

Figure 2. Structures of indole analogs (a−n).

https://doi.org/10.1021/acs.jafc.4c11205
J. Agric. Food Chem. 2025, 73, 7111−7120

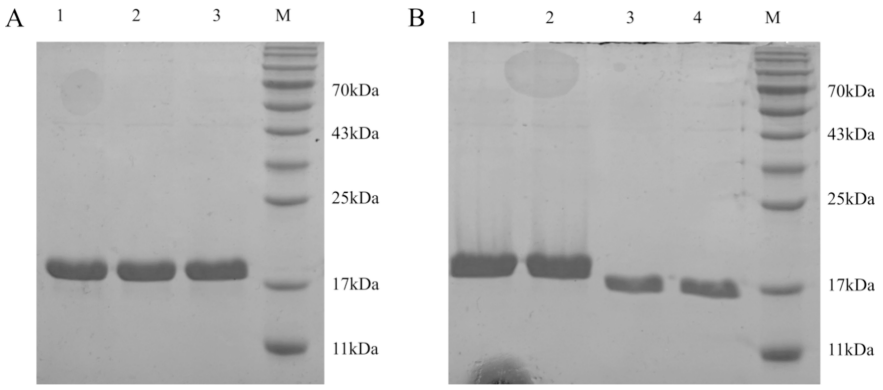

Figure 3. (A) SDS-PAGE gel image of purified *Dm*ATG8a in lanes 1−3 (10 μg). M: protein markers. The loading bufferws 0.25 M Tris-HCl (pH 8.8), 2% SDS, 10% β-mercaptoethanol, and 20% glycerol. The electrophoresis conditions are 100 V for the stacking gel and 120 V for the separating gel. (B) SDS-PAGE gel image of *Dm*ATG8a with His tag in lanes 1−2 (10 μg), of *Dm*ATG8a without His tag in lanes 3−4 (5 μg). M: protein markers. The loading buffer is 0.25 M Tris-HCl (pH 8.8), 2% SDS, 10% β-mercaptoethanol, and 20% glycerol. The electrophoresis conditions are 100 V for the stacking gel and 120 V for the separating gel.

Protein Expression and Purification. The pET32a-*Dm*ATG8a plasmid was transferred into *E. coli* strain BL21 (DE3) and cultured in liquid Luria−Bertani (LB) medium containing ampicillin sodium. The *E. coli* cells were incubated at 37 °C while being gently shaken (200 rpm). When the optical density at 600 nm (OD_{600}) of the liquid LB reached a range of 0.6−1.0, isopropyl-β-D-thiogalactopyranoside (IPTG) was added to a final concentration of 1 mM. Subsequently, the temperature of the shaker was lowered to 20 °C, while maintaining the shaking speed at 200 rpm to induce the expression of the target proteins. After 16 h of induction, the *E. coli* cells were harvested by centrifugation at 6000 *g* and 4 °C for a duration of 15 min. The resulting *E. coli* pellet was then resuspended in 45 mL of lysis buffer (50 mM Tris-HCl, 300 mM NaCl, pH 7.5) and sonicated with a sonicator (Scientz-iid, Scientz) at 35% amplitude for 50 min, with a working cycle of 6 s and pause for 4 s. After sonication, the bacterial solution changed from turbid to clear. The mixture was then centrifuged at 10,760 *g* and 4 °C for 35 min to isolate the supernatant.

The HisTrap HP column (Cytiva, Marlborough, WA) was equilibrated with the binding buffer (50 mM Tris-HCl, 300 mM NaCl, pH 7.5, 20 mM imidazole). The supernatant containing the *Dm*ATG8a protein was injected onto the HisTrap HP column. The column equipped on an AKTA purifier system (GE, Boston, MA) was rinsed for 10 min with the binding buffer at the flow rate to 3 mL/min to remove nontarget proteins. The target proteins were rinsed from the column by gradually increasing the gradient of elution buffer (50 mM Tris-HCl, 300 mM NaCl, pH 7.5, 400 mM imidazole) in 50 mL centrifuge tubes. The elution was concentrated to 10 mL by using ultrafiltration tubes (Amicon Ultra 15 mL). The tobacco etch virus (TEV) protease was added at a mass ratio of 10:1 (target proteins to TEV), and the digestion was carried out overnight at 4 °C. The proteins were injected into the column to remove His-tagged proteins, the effluent was collected. Further purification was performed on a size-exclusion chromatographic column (Superdex 200 pg, Cytiva). The protein solution was concentrated to a volume of 2 mL and subsequently introduced into a loop ring. A desalting buffer (20 mM Tris-HCl, 300 mM NaCl, pH = 7.5) was used to elute the target proteins. The molecular weight and purity of the proteins were verified via 15% sodium dodecyl sulfate-polyacrylamide gel electrophoresis (SDS-PAGE).

Crystallization and Data Processing. *Dm*ATG8a was concentrated to 18 mg/mL in an ultrafiltration tube. The crystallization conditions of *Dm*ATG8a were screened at 18 °C with crystallization kits according to the seated drop vapor diffusion method.[40] Crystals were obtained after 2 days under pool conditions of 0.1 M Bis-Tris pH 6.5, 26 (W/V) PEG MME 5000 (Figure S1). High-quality crystals were equilibrated in an additional pooling solution containing 15% glycerol before being snap-frozen in liquid nitrogen. The final data, with a resolution of 1.369 Å, were collected at the Shanghai Synchrotron Light Source BL17U1 at a wavelength of 0.97918 Å at a temperature of 100 K.

Structure Resolution and Refinement. The crystal data were processed with X-ray Detector Software, revealing a space group of P21 and unit cell dimensions of a = 32.45 Å, b = 58.99 Å, and c = 68.85 Å. The GABARAP (PDB ID: 1GNU) was used as the starting model.[41] Molecular replacement was performed with Phenix software,[42] which provided the initial structural information and electron density maps of the crystals. Finally, the high-resolution crystal structures were manually refined using Coot and Phenix software.[43] The structure has been deposited in the Protein Data Bank with the accession code 9JJD.

Interaction between 6-Fluoroindole and *Dm*ATG8a. The haloindoles and tryptophan were prepared at a concentration of 2 mM and then diluted to 16 different concentrations ranging from 0.06 μM to 2000 μM in polymerase chain reaction (PCR) tubes. *Dm*ATG8a was fluorescently labeled according to the operation steps of the Protein Labeling Kit (RED-NHS second Generation). A 10 μL aliquot of the fluorescently labeled *Dm*ATG8a was added to the PCR tubes containing different compound concentrations. The tubes were placed in the dark for 5 min and then loaded separately into capillary tubes. The binding affinity of the compounds to *Dm*ATG8a was assessed with a Monolith NT 115 (Nano Temper Technologies, Germany).[44−46]

Molecular Docking. The structures of the target compounds were acquired from the PubChem database (https://pubchem.ncbi.nlm.nih.gov/). The compounds were then flexibly docked to *Dm*ATG8a using Autodock Vina 1.1.2 following previously established methods.[47] Conformational docking was performed with PyMOL software. The resulting patterns were plotted.

Purification of *Dm*ATG8a Mutants and Their Interactions with 6-Fluoroindole. The molecular docking results indicated that the hydrogen atom of 6-fluoroindole interacts with the oxygen atom of lysine (K48) of *Dm*ATG8a. Consequently, a site-directed mutation was introduced to replace K48 with alanine (A48). The *Dm*ATG8a mutant sequence was then subcloned into the pET-32a vector, and the protein was transformed, expressed, purified, and desalted according to the methods described previously. MST was conducted to evaluate the binding capacity of the mutant proteins to 6-fluoroindole.

Insecticidal Activity. The insecticidal activity of 6-fluoroindole, which exhibited a high affinity with *Dm*ATG8a, was assessed with a combined toxicity method of gastric poisoning and contact.[48] A section of filter paper was positioned within a 9 cm Petri dish and moistened with 0.8 mL of the solution containing various concentrations of 6-fluoroindole. Apple slices were cut, soaked in the solution for 1 min, and then placed into the Petri dish. Approximately twenty 2-day-old adult flies were gently transferred

https://doi.org/10.1021/acs.jafc.4c11205
J. Agric. Food Chem. 2025, 73, 7111−7120

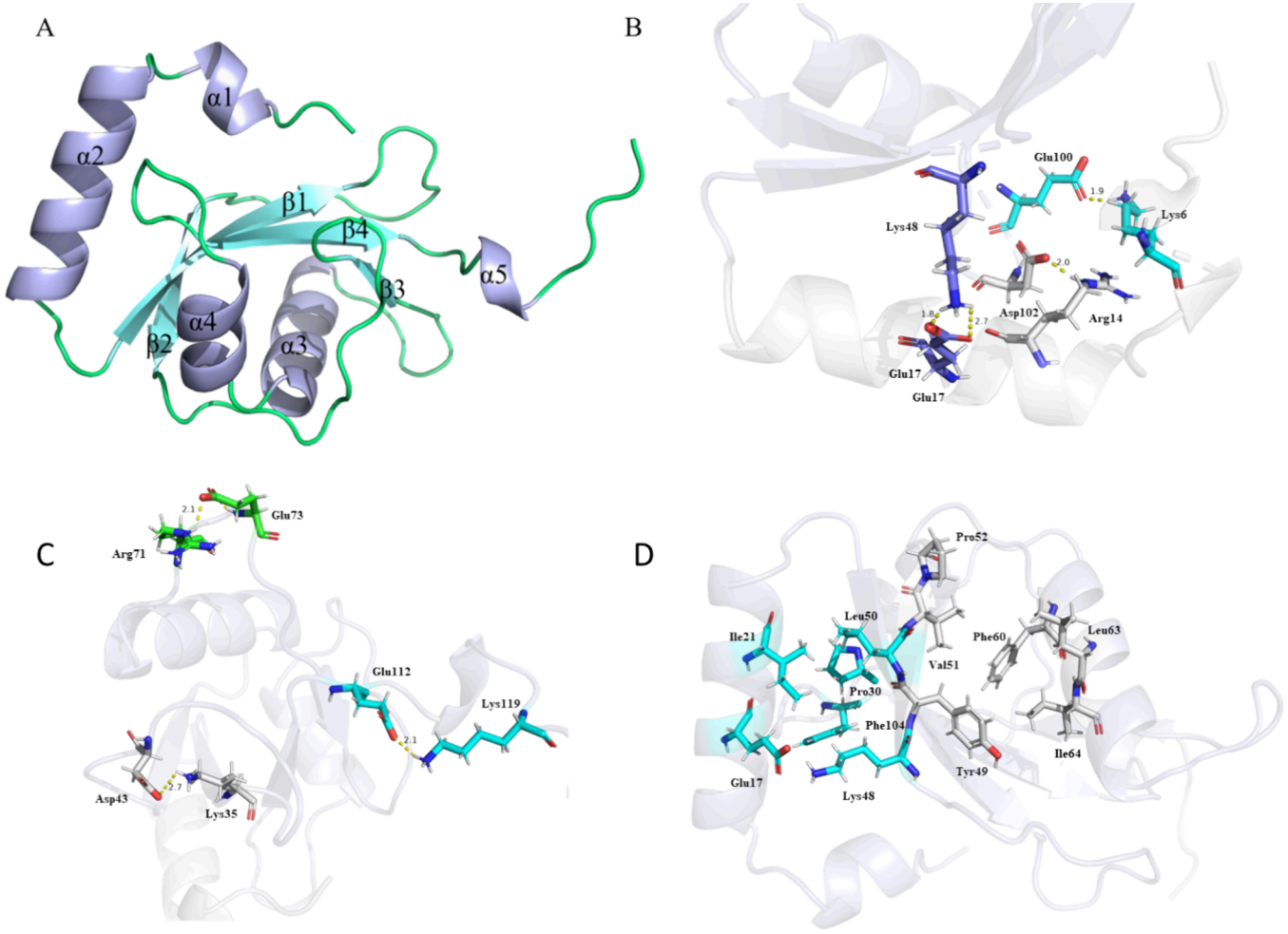

Figure 4. (A) Overall structure of *Dm*ATG8a. α-Helices depicted in purple and β-folding strands shown in blue. (B) Interactions between the ubiquitin fold and the N-terminal helices are depicted, with the N-terminal helices shown in white and the ubiquitin fold in purple. The residues involved in these interactions are marked. (C) Interactions occurring within the ubiquitin fold are illustrated, with the relevant residues also labeled. (D) The two active cavities of *Dm*ATG8a are presented. With residues in the HP1 cavity are shown in blue and those in the HP2 cavity are shown in white.

into the Petri dish using a size 0 brush. Each treatment was triplicate, with water serving as the negative control and avermectin (a potent insecticidal activity against adult fruit flies[49]) as the positive control. Following treatment, the adults were incubated in an incubator set at 24 ± 1 °C, with a humidity of 75 ± 5%, and a photoperiod of 16 h of light and 8 h of dark. The brush was used to lightly touch the insects. If the insect did not move, the insect was considered died. Mortality was observed and recorded after 24 h.

RESULTS AND DISCUSSION

Expression and Purification of Target Protein. After purification with a HisTrap HP column, SDS-PAGE gel analysis revealed a distinct band near 19 kDa (Figure 3A), which was consistent with the predicted size. After TEV protease digestion, the target protein band decrease in size (Figure 3B), indicating the successful removal of the His tag.

Overall Crystal Structure. The crystal structure of *Dm*ATG8a has been refined to a resolution of 1.36 Å (see Table S1 and Figure S2 for more information). The *Dm*ATG8a crystal comprises 121 amino acids and 130 water molecules, featuring a total of five α-helices (α1-α5) and four β-folding strands (β1-β4), with the β-folding strands positioned centrally and the α-helices were distributed on either side (Figure 4A). The overall structure consists of two parts, one is the N-terminal α-helix region (α1, α2), and the other is the core region of the ubiquitination fold (consisting of three α-helixes (α3, α4, and α5)) and four β-folded strands (β1-β4). The α1 and α2 helices are tightly associated with the core region of the ubiquitination fold, stabilized by three salt bridges: Lys6 − Glu100, Arg14 − Asp102, and Glu17 − Lys48 (Figure 4B). Additionally, there are three sets of salt bridges in the core region of the ubiquitination fold of *Dm*ATG8a, namely Lys35 − Asp43, Arg71 − Glu73, and Glu112 − Lys119, which contribute to the stabilization of the region (Figure 4C). All reported ATG8 proteins contain two hydrophobic pockets. *Dm*ATG8a also contained two hydrophobic pockets. Pocket 1 lied between α-helix 2 and the ubiquitination fold region, comprising Glu17, Ile21, Pro30, Lys48, Leu50 and Phe104, Pocket 2 was located within the ubiquitination fold region and included Tyr49, Val51, Pro52, Phe60, Leu63, and Ile64 (Figure 4D). As previously reported,[50,51] the ATG8 protein binds proteins containing the LC3 interaction region (LIR) via two pockets. The LIR sequence contains four main amino acids (ΦXXΨ), Φ for aromatic amino acids (W/F/Y), XX for arbitrary amino acids and Ψ for aliphatic amino acids (L/V/I). Pocket 1 predominantly binds aromatic amino acids, while pocket 2 binds aliphatic amino acids. Within the three

https://doi.org/10.1021/acs.jafc.4c11205
J. Agric. Food Chem. 2025, 73, 7111−7120

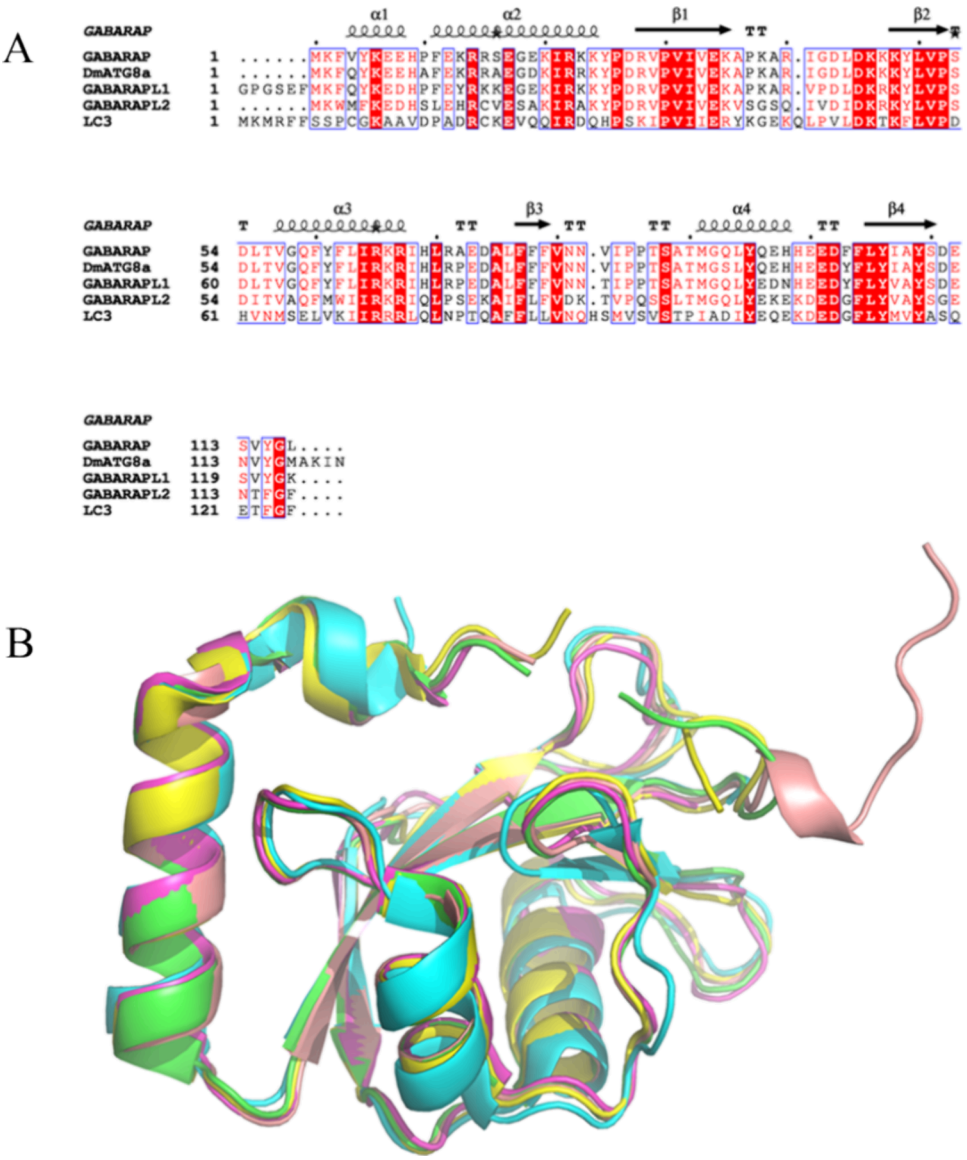

Figure 5. Comparison of five similar structures. (A) Structure-based sequence alignment of GABARAP (88.73% identity), GABARAPL1 (77.95% identity), GABARAPL2 (55.37% identity), and LC3 (28.68% identity) with *Dm*ATG8a. Alignments were performed with the program ESPript. (B) A superposition of the overall structures shows *Dm*ATG8a (pink) alongside GABARAP (green), GABARAPL1 (blue), GABARAPL2 (purple), and LC3 (yellow).

aromatic amino acids (W/F/Y) that can bind to pocket 1, tryptophan occupies a dominant position, based on previous findings, it was later found that indole analogs (structurally similar to tryptophan) also have an affinity for the HP1 pocket of the ATG8 protein.[35]

We also analyzed the surface charge of the active cavity of *Dm*ATG8a. By using Pymol software to generate the surface charge map of the active cavities of *Dm*ATG8a, where blue indicates positive charge and red indicates negative charge, and the intensity of the color represents the charge density (Figure S3), This suggests that the cavity carries a significant amount of positive charge. It is hypothesized that when this cavity binds other proteins, it intends to interact with residues carrying negative charges. This finding provides a novel direction for our subsequent search for other structures that may bind to the active cavity of ATG8.

Structural Comparison. Multiple sequence comparisons of crystallized ATG8 homologues revealed that the amino acid sequences of ATG8 protein are highly conserved from mammals to insects. When the amino acid sequence of *Dm*ATG8a was compared with those of GABARAP (PDB code 1GNU),[41] GABARAPL1 (PDB code 2R2Q), GABARAPL2 (PDB code 7LK3),[52] and LC3 (PDB code 1UGM),[53] the sequence similarities were 88.43%, 77.95%, 55.37% and 28.68%, respectively (Figure 5A). The structures of *Dm*ATG8a were overlaid with those of GABARAP, GABARAPL1, GABARAPL2, and LC3, yielding root-mean-square deviation (RMSD) values of 0.422, 0.448, 0.527, and 0.96 Å, respectively (Figure 5B). All currently resolved ATG8 family proteins consist of four α-helices and four β-folding strands, however, the *Dm*ATG8a protein uniquely contains five α-helices and four β-folding strands, with α5 located in the core region of the ubiquitylated fold and directly connected to β4. The results indicate the specificity of the structure of *Dm*ATG8a.

Binding Constants of Test Compounds to *Dm*ATG8a. MST was used to evaluate the binding affinity of compounds a-

https://doi.org/10.1021/acs.jafc.4c11205
J. Agric. Food Chem. 2025, 73, 7111−7120

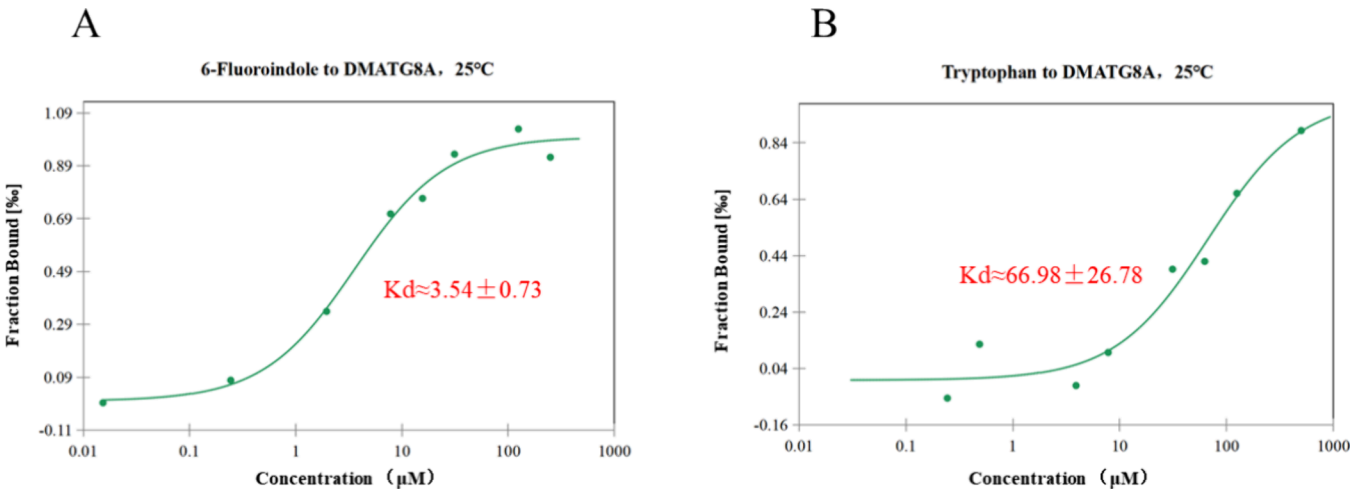

Figure 6. MST binding curves of (A) 6-fluoroindole with *Dm*ATG8a at 25 °C. (B) Tryptophan with *Dm*ATG8a at 25 °C.

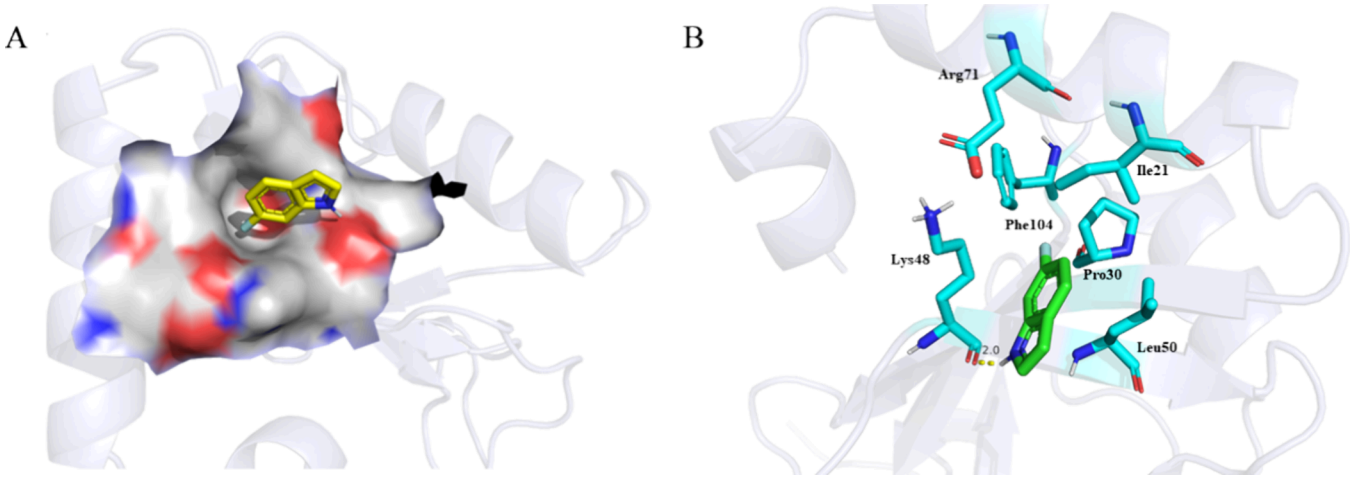

Figure 7. Molecular docking result of 6-fluoroindole and *Dm*ATG8a. (A) Cavity binding sites of *Dm*ATG8a and 6-fluoroindole. (B) Binding residue sites of *Dm*ATG8a and 6-fluoroindole.

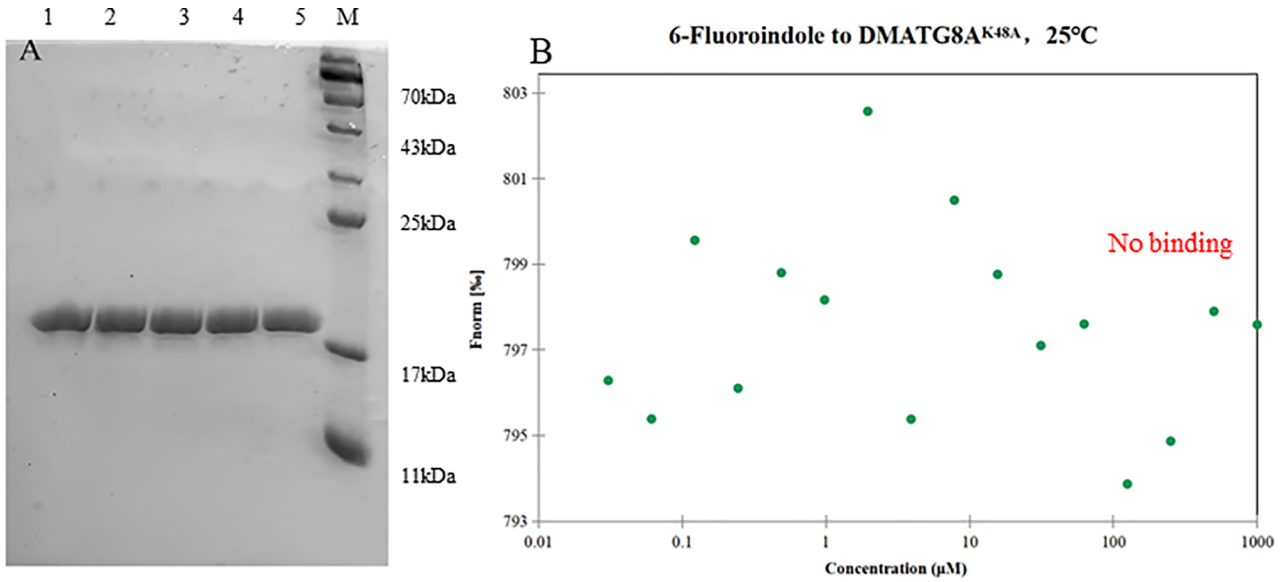

Figure 8. (A) SDS-PAGE gel image of purified *Dm*ATG8A^{K48A} in lanes 1−5 (10 μg). M: protein markers. The loading buffer is 0.25 M Tris-HCl (pH 8.8), 2% SDS, 10% β-mercaptoethanol, and 20% glycerol. The electrophoresis conditions are 100 V for the stacking gel and 120 V for the separating gel; and (B) MST results of 6-fluoroindole with *Dm*ATG8A^{K48A}.

https://doi.org/10.1021/acs.jafc.4c11205
J. Agric. Food Chem. 2025, 73, 7111−7120

Table 1. LC_{50} Values of Abamectin and 6-Fluoroindole against *D. melanogaster*

Compound	y = a+bx	R (Correlation coefficient)	LC_{50} (mg/L)	95% confidence interval (mg/L)
6-fluoroindole	y = 0.4171x-22.587	0.98	169	142−196
abamectin	y = 0.5718x+27.13	0.98	30.5	9.56−53.2

n (Figure S4) and tryptophan to *Dm*ATG8a. 6-Fluoroindole demonstrated strong binding and exhibited a well-defined binding curve, with a K_d value of 3.54 μmol/L, being approximately 19-fold lower than tryptophan's K_d value of 66.98 μmol/L (Figure 6). This result indicates that 6-fluoroindole had a stronger binding affinity for *Dm*ATG8a than tryptophan in vitro. A previous study[35] has shown that the ATG8 protein has a specific binding site for indole analogs, which may be the reason for the strong binding of 6-fluoroindole to *Dm*ATG8a.

Molecular Docking of 6-Fluoroindole with *Dm*ATG8a. Probing the binding sites of proteins and small molecules is crucial for inhibitor design. The molecular docking results indicated formation of a hydrogen bond between 6-fluoroindole and Lys48 in the HP1 of *Dm*ATG8a (Figure 7).

Through molecular docking, we evaluated the interaction between 6-fluoroindole and *Dm*ATG8a and investigated the involvement of key amino acids. The preliminary experimental results show formation of a hydrogen bond between 6-fluoroindole and Lys48, resulting in a high binding force. Mutation of Lys48 − Ala48 can verify whether the above assessment is correct. Therefore, in the remainder work, we studied the binding force between the mutant *Dm*ATG8a^{K48A} and 6-fluorooindole.

Lack of Interaction between *Dm*ATG8a^{K48A} and 6-Fluoroindole. There was no binding between *Dm*ATG8A^{K48A} and 6-fluoroindole. This result supported the notion that Lys48 was a key amino acid for the interaction between 6-fluoroindole and *Dm*ATG8a (Figure 8).

Activity of Target Compounds against *D. melanogaster*. Based on the binding results, 6-fluoroindole that exhibited strong binding activity with *Dm*ATG8a was selected for *in vivo* experiments against *D. melanogaster*. 6-Fluoroindole and avermectin demonstrated 100% insecticidal activity against *D. melanogaster* at a concentration of 500 μg/mL. However, as the concentration decreased, the insecticidal activity of 6-fluoroindole showed a significant decrease, only 24% of *D. melanogaster* died at a concentration of 125 μg/mL. This sharp dose−response relationship suggests the essentiality of *Dm*ATG8a to *D. melanogaster* and its high potential as an insecticidal target. In comparison, the positive control avermectin exhibited greater insecticidal activity than 6-fluoroindole, resulting in 33% mortality in *D. melanogaster* even at a concentration of 15 μg/mL. The final half-maximal lethal concentration (LC_{50}) of 6-fluoroindole was 169 μg/mL, while the LC_{50} of avermectin was 30.5 μg/mL (Table 1). This suggests that structural optimization of 6-fluoroindole may enhance its potency.

The identification of new drug targets is crucial for managing field pests and reducing the damage they cause to crops. ATG8 is a core component of the autophagy process.[29] It interacts with various autophagy-related proteins (e.g., ULK1, TBC1D25, reticulin, ATG4B, and ATG7) and cargo receptor proteins (e.g., p62 NBR1 and NDP52), thereby influencing cellular autophagy,[29] which is vital for normal growth and development of organisms. $GABA_A$ receptors are targets for a variety of drugs, including anesthetics, sedatives, hypnotics and antidepressants.[54−56] GABARAP can promote the aggregation of $GABA_A$ receptors, transport them to the cell membrane, and affect the dynamics of gated ion channels, which has a great influence on some physiological functions of $GABA_A$ receptors.[9, 10]

Most existing studies on ATG8 proteins, however, have primarily concentrated on mammals, with relatively few investigations focused on insects. The study of ATG8 proteins in insects can not only serve as a reference for the study of ATG8 in other higher animals including humans, but also as a target site for the development and the control of insect pests.

A majority of traditional insecticides target the nervous system such as the $GABA_A$ receptors of insects. The GABAergic insecticides inhibit the $GABA_A$ receptor but not ATG8. As an autophagy-related protein, *Dm*ATG8a participates in the autophagy process of insects.[11] Autophagy is an intracellular degradation and recycling mechanism, that is vital for maintaining intracellular homeostasis, responding to various stress conditions, and facilitating the metamorphic development of insects.[57] Insecticides targeting *Dm*ATG8a can disrupt the autophagy process in insects, thereby affecting their normal physiological functions and neuronal integrity and consequentially achieving pest control objectives. This mechanism of action differs from and may reduce cross-resistance with the traditional insecticides such as GABAergic insecticides.

D. melanogaster has been used for more than a century as a model organism to study a wide range of life science questions, such as drug discovery and target discovery.[28,29] Previous studies have found that knocking out ATG8a in *D. melanogaster* greatly reduces lifespan and affect normal physiological functions and neuronal integrity.[32] In addition, our previous study[34] determined specific interaction between methyl eugenol and recombinant GABARAP from the western flower thrips *Frankliniella occidentalis*. Therefore, *D. melanogaster* was used as a good material to study whether insect ATG8 protein has the potential to be an insecticide target.

*Dm*ATG8a is composed of five α-helices and four β-folding strands. Compared with the human ATG8 protein with only four α-helices and four β-folding strands, the α5 of *D. melanogaster* may play an important role in $GABA_A$ receptors and autophagy. Further exploration of the function of the α5 region is an interesting and important direction for future research.

The insect ATG8 is being studied as a potential pesticide target. For example, methyl eugenol can interact with Tyr61 residue of ATG8 protein of thrips, resulting in the death of thrips (with an LC_{50} values was 1.1 mg/L).[34] *Dm*ATG8a plays an important role in the normal physiological function of *D. melanogaster* and seems to be a potential target for insecticides. Based on the structure of *Dm*ATG8a, we determined the binding affinities of a series of halogenated indole compounds to the active cavity HP1 of *Dm*ATG8a. The results indicated that 6-fluoroindole has a strong binding ability. The ATG8 protein mainly interacts with other proteins through two cavities, HP1 and HP2. The molecular docking results showed that the amino group of 6-fluoroindole forms hydrogen bonds

https://doi.org/10.1021/acs.jafc.4c11205
J. Agric. Food Chem. 2025, 73, 7111−7120

with K48 of ATG8, and the benzene ring part of 6-fluoroindole is inserted into the HP1 cavity of ATG8. Therefore, we speculate that 6-fluoroindole may inhibit the interaction between ATG8 and other proteins by occupying the active site of HP1, thereby preventing the residues of other proteins from binding to the HP1 cavity of ATG8 and malfunctioning ATG8 to perform normal physiological roles.

This study represents the first comprehensive analysis of the crystal structure of *Dm*ATG8a, revealing its distinctiveness from the reported structures of most ATG8 proteins. It offers a novel perspective for the structural research of the ATG8 proteins, facilitating a deeper understanding of the structural diversity and functional specificity of this protein in different organism species. This is the second study to conduct potential insecticide target research on insect ATG8 proteins.[34] We evaluated the insecticidal activity of 6-fluoroindole to *D. melanogaster*, which opens a new avenue for the development of novel insecticides. However, the structure of 6-fluoroindole requires further optimization to enhance its biological activity. The findings warrant an interest in studying ATG8 from other insect and organism species for structural uniqueness and selectivity as an insecticidal action target.

■ ASSOCIATED CONTENT

Supporting Information

The Supporting Information is available free of charge at https://pubs.acs.org/doi/10.1021/acs.jafc.4c11205.

Crystal parameters, data-collection and structure-refinement statistics (Table S1); image of crystals of DmATG8a (1−121) (Figure S1); Ramachandran plot of *Dm*ATG8a (Figure S2); surface charge map of the active cavities of HP1 and HP2 of DmATG8a (Figure S3); and MST binding curves of preliminary screening of interactions between DmATG8a and titled compounds (Figure S4) (PDF)

■ AUTHOR INFORMATION

Corresponding Authors

Xiangyang Li − *State Key Laboratory of Green Pesticide, Key Laboratory of Green Pesticide and Agricultural Bioengineering, Ministry of Education, Guizhou University, Guiyang 550025, China;* orcid.org/0000-0002-1502-1811; Email: xyli1@gzu.edu.cn

Qing X. Li − *Department of Molecular Biosciences and Bioengineering, University of Hawaii at Manoa, Honolulu 96822 Hawaii, United States; Hawaii Pacific Neuroscience, Honolulu 96817 Hawaii, United States;* orcid.org/0000-0003-4589-2869; Email: qingl@hawaii.edu

Authors

Shanqi Zhang − *State Key Laboratory of Green Pesticide, Key Laboratory of Green Pesticide and Agricultural Bioengineering, Ministry of Education, Guizhou University, Guiyang 550025, China*

Xin Luo − *State Key Laboratory of Green Pesticide, Key Laboratory of Green Pesticide and Agricultural Bioengineering, Ministry of Education, Guizhou University, Guiyang 550025, China*

Xiu Yuan − *Department of Molecular Biosciences and Bioengineering, University of Hawaii at Manoa, Honolulu 96822 Hawaii, United States*

Danxia Wu − *State Key Laboratory of Green Pesticide, Key Laboratory of Green Pesticide and Agricultural Bioengineering, Ministry of Education, Guizhou University, Guiyang 550025, China*

Jing Liu − *State Key Laboratory of Green Pesticide, Key Laboratory of Green Pesticide and Agricultural Bioengineering, Ministry of Education, Guizhou University, Guiyang 550025, China*

Kunhong Zhao − *State Key Laboratory of Green Pesticide, Key Laboratory of Green Pesticide and Agricultural Bioengineering, Ministry of Education, Guizhou University, Guiyang 550025, China*

Youwei Xu − *State Key Laboratory of Green Pesticide, Key Laboratory of Green Pesticide and Agricultural Bioengineering, Ministry of Education, Guizhou University, Guiyang 550025, China*

Jingjiang Zhou − *State Key Laboratory of Green Pesticide, Key Laboratory of Green Pesticide and Agricultural Bioengineering, Ministry of Education, Guizhou University, Guiyang 550025, China*

Complete contact information is available at: https://pubs.acs.org/10.1021/acs.jafc.4c11205

Author Contributions

Shanqi Zhang: experiment design, data collection, and writing the first draft of the manuscript. Youwei Xu, Jingjiang Zhou, Xiangyang Li, and Qing X. Li: conceptualization, supervision, data interpretation, manuscript revisions, and editing. Xin Luo, Danxia Wu, Jing Liu, and Kunhong Zhao: data collection, manuscript review. Jingjiang Zhou and Xiu Yuan: manuscript review.

Notes

The authors declare no competing financial interest.

■ ACKNOWLEDGMENTS

This work was supported in part by the National Natural Science Foundation of China (grant nos. 32330087 and 32172461), Guizhou Province Science and Technology Plan Project, Major Science and Technology Achievement Transformation Project QKH [grant no. (2024)007], Talents of Guizhou Science and Technology Cooperation Platform [grant no. (2021)5623], and the USDA (HAW05020H and HAW05044R).

■ REFERENCES

(1) Godfray, H. C.; Beddington, J. R.; Crute, I. R.; Haddad, L.; Lawrence, D.; Muir, J. F.; Pretty, J.; Robinson, S.; Thomas, S. M.; Toulmin, C. Food security: the challenge of feeding 9 billion people. *Science* **2010**, *327*, 812−8.

(2) Huang, W.; Wei, S.; Zhou, T.; Fan, Z.; Cao, L.; Li, Z.; Guo, S. MCMV-infected maize attracts its insect vector Frankliniella occidentalis by inducing *β*-myrcene. *Front. Plant Sci.* **2024**, *15*, No. 1404271.

(3) Ruark-Seward, C. L.; Bonville, B.; Kennedy, G.; Rasmussen, D. A. Evolutionary dynamics of tomato spotted wilt virus within and between alternate plant hosts and thrips. *Sci. Rep* **2020**, *10*, 15797.

(4) Karabörklü, S.; Azizoglu, U.; Azizoglu, Z. B. Recombinant entomopathogenic agents: a review of biotechnological approaches to pest insect control. *World J. Microbiol. Biotechnol.* **2017**, *34*, 14.

(5) Macias, V. M.; Ohm, J. R.; Rasgon, J. L. Gene Drive for Mosquito Control: Where Did It Come from and Where Are We Headed? *Int. J. Environ. Res. Public Health* **2017**, *14*, 1006.

(6) Wang, H.; Bedford, F. K.; Brandon, N. J.; Moss, S. J.; Olsen, R. W. GABA(A)-receptor-associated protein links GABA(A) receptors and the cytoskeleton. *Nature* **1999**, *397*, 69−72.
(7) Coyle, J. E.; Qamar, S.; Rajashankar, K. R.; Nikolov, D. B. Structure of GABARAP in two conformations: implications for GABA(A) receptor localization and tubulin binding. *Neuron* **2002**, *33*, 63−74.
(8) Chen, L.; Wang, H.; Vicini, S.; Olsen, R. W. The gamma-aminobutyric acid type A (GABAA) receptor-associated protein (GABARAP) promotes GABAA receptor clustering and modulates the channel kinetics. *Proc. Natl. Acad. Sci. USA* **2000**, *97*, 11557−62.
(9) Chen, Z. W.; Chang, C. S.; Leil, T. A.; Olcese, R.; Olsen, R. W. GABAA receptor-associated protein regulates GABAA receptor cell-surface number in Xenopus laevis oocytes. *Mol. Pharm.* **2005**, *68*, 152−9.
(10) Leil, T. A.; Chen, Z. W.; Chang, C. S.; Olsen, R. W. GABAA receptor-associated protein traffics GABAA receptors to the plasma membrane in neurons. *J. Neurosci.* **2004**, *24*, 11429−38.
(11) Mizushima, N. The ATG conjugation systems in autophagy. *Curr. Opin. Cell Biol.* **2020**, *63*, 1−10.
(12) Bassham, D. C. Function and regulation of macroautophagy in plants. *Biochim. Biophys. Acta* **2009**, *1793*, 1397−403.
(13) Floyd, B. E.; Morriss, S. C.; Macintosh, G. C.; Bassham, D. C. What to eat: evidence for selective autophagy in plants. *J. Integr. Plant Biol.* **2012**, *54*, 907−20.
(14) Zhuang, X.; Cui, Y.; Gao, C.; Jiang, L. Endocytic and autophagic pathways crosstalk in plants. *Curr. Opin. Plant Biol.* **2015**, *28*, 39−47.
(15) Liu, Y.; Bassham, D. C. Autophagy: pathways for self-eating in plant cells. *Annu. Rev. Plant Biol.* **2012**, *63*, 215−37.
(16) van Doorn, W. G.; Woltering, E. J. Many ways to exit? Cell death categories in plants. *Trends Plant Sci.* **2005**, *10*, 117−22.
(17) Hayashi-Nishino, M.; Fujita, N.; Noda, T.; Yamaguchi, A.; Yoshimori, T.; Yamamoto, A. A subdomain of the endoplasmic reticulum forms a cradle for autophagosome formation. *Nat. Cell Biol.* **2009**, *11*, 1433−7.
(18) Hailey, D. W.; Rambold, A. S.; Satpute-Krishnan, P.; Mitra, K.; Sougrat, R.; Kim, P. K.; Lippincott-Schwartz, J. Mitochondria supply membranes for autophagosome biogenesis during starvation. *Cell* **2010**, *141*, 656−67.
(19) Ravikumar, B.; Moreau, K.; Jahreiss, L.; Puri, C.; Rubinsztein, D. C. Plasma membrane contributes to the formation of pre-autophagosomal structures. *Nat. Cell Biol.* **2010**, *12*, 747−57.
(20) Kirisako, T.; Ichimura, Y.; Okada, H.; Kabeya, Y.; Mizushima, N.; Yoshimori, T.; Ohsumi, M.; Takao, T.; Noda, T.; Ohsumi, Y. The reversible modification regulates the membrane-binding state of Apg8/Aut7 essential for autophagy and the cytoplasm to vacuole targeting pathway. *J. Cell Biol.* **2000**, *151*, 263−76.
(21) Nakatogawa, H.; Ishii, J.; Asai, E.; Ohsumi, Y. Atg4 recycles inappropriately lipidated Atg8 to promote autophagosome biogenesis. *Autophagy* **2012**, *8*, 177−86.
(22) Ichimura, Y.; Kirisako, T.; Takao, T.; Satomi, Y.; Shimonishi, Y.; Ishihara, N.; Mizushima, N.; Tanida, I.; Kominami, E.; Ohsumi, M.; Noda, T.; Ohsumi, Y. A ubiquitin-like system mediates protein lipidation. *Nature* **2000**, *408*, 488−92.
(23) Mizushima, N.; Noda, T.; Yoshimori, T.; Tanaka, Y.; Ishii, T.; George, M. D.; Klionsky, D. J.; Ohsumi, M.; Ohsumi, Y. A protein conjugation system essential for autophagy. *Nature* **1998**, *395*, 395−8.
(24) Tanida, I.; Mizushima, N.; Kiyooka, M.; Ohsumi, M.; Ueno, T.; Ohsumi, Y.; Kominami, E. Apg7p/Cvt2p: A novel protein-activating enzyme essential for autophagy. *Mol. Biol. Cell* **1999**, *10*, 1367−79.
(25) Noda, N. N.; Fujioka, Y.; Hanada, T.; Ohsumi, Y.; Inagaki, F. Structure of the Atg12-Atg5 conjugate reveals a platform for stimulating Atg8-PE conjugation. *EMBO Rep* **2013**, *14*, 206−11.
(26) Taherbhoy, A. M.; Tait, S. W.; Kaiser, S. E.; Williams, A. H.; Deng, A.; Nourse, A.; Hammel, M.; Kurinov, I.; Rock, C. O.; Green, D. R.; Schulman, B. A. Atg8 transfer from Atg7 to Atg3: a distinctive E1−E2 architecture and mechanism in the autophagy pathway. *Mol. Cell* **2011**, *44*, 451−61.
(27) Johansen, T.; Lamark, T. Selective Autophagy: ATG8 Family Proteins, LIR Motifs and Cargo Receptors. *J. Mol. Biol.* **2020**, *432*, 80−103.
(28) Shahzad, U.; Taccone, M. S.; Kumar, S. A.; Okura, H.; Krumholtz, S.; Ishida, J.; Mine, C.; Gouveia, K.; Edgar, J.; Smith, C.; Hayes, M.; Huang, X.; Derry, W. B.; Taylor, M. D.; Rutka, J. T. Modeling human brain tumors in flies, worms, and zebrafish: From proof of principle to novel therapeutic targets. *Neuro Oncol* **2021**, *23*, 718−731.
(29) Gasque, G.; Conway, S.; Huang, J.; Rao, Y.; Vosshall, L. B. Small molecule drug screening in Drosophila identifies the 5HT2A receptor as a feeding modulation target. *Sci. Rep* **2013**, *3*, No. 02120.
(30) McPhee, C. K.; Baehrecke, E. H. Autophagy in Drosophila melanogaster. *Biochim. Biophys. Acta* **2009**, *1793*, 1452−60.
(31) Zinke, I.; Schütz, C. S.; Katzenberger, J. D.; Bauer, M.; Pankratz, M. J. Nutrient control of gene expression in Drosophila: microarray analysis of starvation and sugar-dependent response. *EMBO J.* **2002**, *21*, 6162−73.
(32) Xu, Y.; Liu, W.; Sun, Z.; Yu, Y.; Yang, T.; Lu, X.; Zhang, G.; Jiao, J.; Duan, X. The two autophagy-related proteins 8a and 8b play distinct physiological roles in Drosophila. *Genomics* **2024**, *116*, No. 110853.
(33) Woo, J.; Jung, S.; Kim, S.; Li, Y.; Chung, H.; Roubtsova, T. V.; Zhang, H.; Caseys, C.; Kliebenstein, D.; Kim, K. N.; Bostock, R. M.; Lee, Y. H.; Dickman, M. B.; Choi, D.; Park, E.; Dinesh-Kumar, S. P. Attenuation of phytofungal pathogenicity of Ascomycota by autophagy modulators. *Nat. Commun.* **2024**, *15*, 1621.
(34) Wang, L.; Huang, M. X.; Wu, Z.; Huang, M.; Yan, Y. L.; Song, B. A.; Li, X. Y.; Li, Q. X. Methyl eugenol binds recombinant gamma-aminobutyric acid receptor-associated protein from the western flower thrips Frankliniella occidentalis. *J. Agric. Food Chem.* **2022**, *70*, 4871−4880.
(35) Thielmann, Y.; Mohrlüder, J.; Koenig, B. W.; Stangler, T.; Hartmann, R.; Becker, K.; Höltje, H. D.; Willbold, D. An indole-binding site is a major determinant of the ligand specificity of the GABA type A receptor-associated protein GABARAP. *Chembiochem* **2008**, *9*, 1767−75.
(36) Costa, Â. C. F.; Cavalcanti, S. C. H.; Santana, A. S.; Lima, A. P. S.; Santana, E. D. R.; Brito, T. B.; Oliveira, R. R. B.; Macêdo, N. A.; Cristaldo, P. F.; Bacci, L. Formicidal activity of indole derivatives on Atta opaciceps (Borgmeier): Lethal, behavioural and locomotive effects. *J. Appl. Entomol* **2019**, *143*, 58−68.
(37) Costa, Â. C. F.; Cavalcanti, S. C. H.; Santana, A. S.; Lima, A. P. S.; Brito, T. B.; Oliveira, R. R. B.; Macêdo, N. A.; Cristaldo, P. F.; Araújo, A. P. A.; Bacci, L. Insecticidal activity of indole derivatives against Plutella xylostella and selectivity to four non-target organisms. *Ecotoxicology* **2019**, *28*, 973−982.
(38) Lu, A.; Wang, T.; Hui, H.; Wei, X.; Cui, W.; Zhou, C.; Li, H.; Wang, Z.; Guo, J.; Ma, D.; Wang, Q. Natural Products for Drug Discovery: Discovery of Gramines as Novel Agents against a Plant Virus. *J. Agric. Food Chem.* **2019**, *67*, 2148−2156.
(39) Lin, L. B.; Gao, Y. Q.; Han, R.; Xiao, J.; Wang, Y. M.; Zhang, Q.; Zhai, Y. J.; Han, W. B.; Li, W. L.; Gao, J. M. Alkylated Salicylaldehydes and Prenylated Indole Alkaloids from the Endolichenic Fungus Aspergillus chevalieri and Their Bioactivities. *J. Agric. Food Chem.* **2021**, *69*, 6524−6534.
(40) Hou, H.; Shi, M.; Hu, S. Y.; Ahmad, F.; Zhang, B.; Chen, Z. H.; Yin, D. C. A systematic comparison of sitting and hanging-drop crystallization using traditional and cross-diffusion microbatch crystallization plates. *J. Cryst. Growth* **2019**, *521*, 1−8.
(41) Knight, D.; Harris, R.; McAlister, M. S.; Phelan, J. P.; Geddes, S.; Moss, S. J.; Driscoll, P. C.; Keep, N. H. The X-ray crystal structure and putative ligand-derived peptide binding properties of gamma-aminobutyric acid receptor type A receptor-associated protein. *J. Biol. Chem.* **2002**, *277*, 5556−61.
(42) Adams, P. D.; Afonine, P. V.; Bunkóczi, G.; Chen, V. B.; Davis, I. W.; Echols, N.; Headd, J. J.; Hung, L. W.; Kapral, G. J.; Grosse-Kunstleve, R. W.; McCoy, A. J.; Moriarty, N. W.; Oeffner, R.; Read, R. J.; Richardson, D. C.; Richardson, J. S.; Terwilliger, T. C.; Zwart, P.

https://doi.org/10.1021/acs.jafc.4c11205
J. Agric. Food Chem. 2025, 73, 7111−7120

H. PHENIX: a comprehensive Python-based system for macromolecular structure solution. *Acta Crystallogr. D Biol. Crystallogr.* **2010**, *66*, 213−21.
(43) Emsley, P.; Lohkamp, B.; Scott, W. G.; Cowtan, K. Features and development of Coot. *Acta Crystallogr. D Biol. Crystallogr.* **2010**, *66*, 486−501.
(44) Wang, C.; Ma, G. M.; Zhang, S. Q.; Zhao, K. H.; Li, X. Y. Study on the binding of ningnanmycin to the helicase of Tobamovirus virus. *Pestic. Biochem. Physiol.* **2023**, *194*, No. 105494.
(45) Bai, Q.; Jiang, J.; Luo, D.; Huang, Y.; Huang, M.; Zhao, G.; Wang, Z.; Li, X. Cysteine protease domain of potato virus Y: The potential target for urea derivatives. *Pestic. Biochem. Physiol.* **2023**, *189*, No. 105309.
(46) Wang, D.; Huang, M.; Gao, D.; Chen, K.; Xinxie; Xu, W.; Li, X. Screening anti-TMV agents targeting tobacco mosaic virus helicase protein. *Pestic. Biochem. Physiol.* **2020**, *166*, No. 104449.
(47) Morris, G. M.; Lim-Wilby, M. Molecular docking. *Methods Mol. Biol.* **2008**, *443*, 365−82.
(48) Ding, Q.; Wang, Y. T.; Liu, J. J.; Shi, X. Y.; Gao, X. W.; Song, G. L. Monitoring the resistance of field populations of oradysia odoriphaga Yangt Zhang in the main leek producing areas in China. *J. Appl. Entomol* **2016**, *53*, 1242−1249.
(49) Tian, W. J.; Shi, H. Y.; Shi, J. H.; Ding, X.; Zhang, J. A comparative study on control effects of fruit flies by different drugs. *Biol. Bull.* **2021**, *56*, 47−50.
(50) Noda, N. N.; Kumeta, H.; Nakatogawa, H.; Satoo, K.; Adachi, W.; Ishii, J.; Fujioka, Y.; Ohsumi, Y.; Inagaki, F. Structural basis of target recognition by Atg8/LC3 during selective autophagy. *Genes Cells* **2008**, *13*, 1211−8.
(51) Birgisdottir, Å. B.; Lamark, T.; Johansen, T. The LIR motif - crucial for selective autophagy. *J. Cell. Sci.* **2013**, *126*, 3237−47.
(52) Scicluna, K.; Dewson, G.; Czabotar, P. E.; Birkinshaw, R. W. A new crystal form of GABARAPL2. *Acta Crystallogr. F Struct Biol. Commun.* **2021**, *77*, 140−147.
(53) Sugawara, K.; Suzuki, N. N.; Fujioka, Y.; Mizushima, N.; Ohsumi, Y.; Inagaki, F. The crystal structure of microtubule-associated protein light chain 3, a mammalian homologue of Saccharomyces cerevisiae Atg8. *Genes Cells* **2004**, *9*, 611−8.
(54) Barnard, E. A.; Skolnick, P.; Olsen, R. W.; Mohler, H.; Sieghart, W.; Biggio, G.; Braestrup, C.; Bateson, A. N.; Langer, S. Z. Subtypes of gamma-aminobutyric acid A receptors: classification on the basis of subunit structure and receptor function. *Pharmacol. Rev.* **1998**, *50*, 291−313.
(55) Olsen, R. W.; Sieghart, W. Subtypes of gamma-aminobutyric acid(A) receptors: classification on the basis of subunit composition, pharmacology, and function. *Pharmacol. Rev.* **2008**, *60*, 243−60.
(56) Smart, T. G.; Stephenson, F. A. A half century of γ-aminobutyric acid. *Brain Neurosci Adv.* **2019**, *3*, No. 2398212819858249.
(57) Parthasarathy, R.; Palli, S. R. Developmental and hormonal regulation of midgut remodeling in a lepidopteran insect. *Heliothis virescens. Mech Dev* **2007**, *124*, 23−34.

https://doi.org/10.1021/acs.jafc.4c11205
J. Agric. Food Chem. 2025, 73, 7111−7120